Granular Flow Modeling of Galvanized Steel Scrap Injection into the HIsarna Iron-Making Reactor

Hosseini, Ashkan; Georgopoulos, Evangelos; Dihman, Vinod; Hage, Johannes; Meijer, Koen; Zeilstra, Christiaan; Offerman, Erik; Yang, Yongxiang

Important note
To cite this publication, please use the final published version (if applicable).
Please check the document version above.

Granular Flow Modeling of Galvanized Steel Scrap Injection into the HIsarna Iron-Making Reactor

Ashkan Hosseini,* Evangelos Georgopoulos, Vinod Dihman, Johannes Hage, Koen Meijer, Christiaan Zeilstra, Erik Offerman, and Yongxiang Yang

Galvanized steel scrap flow and injection into the HIsarna reactor are investigated using discrete element method (DEM). The scrap particle is fed into the reactor through an inclined chute and hits the slag surface where the zinc content is evaporated and solid particles melt. A DEM model is setup and validated using experimental data obtained from the exact plant-scale chute geometry and scrap particles. Using the DEM model, the effect of chute inclination, injection elevation, injection mode (batch and continuous), batch size, and flowrate on particle distribution and exerted pressure on the slag surface are investigated. It is found that continuous mode of injection is the most suitable method to increase the spread of particles and also to reduce the exerted pressure on the slag surface. Placing dent-like obstacles at the tip of the chute significantly increases the impact area, especially for batchwise injection, thus reducing force and pressure on the slag surface that minimizes the risk of liquid splash. Larger particle impact area is also beneficial to obtain higher zinc evaporation rate from particle surface and also to minimize the slag surface temperature disturbance.

1. Introduction

The HIsarna process is a new and breakthrough smelting reduction technology for the production of liquid hot metal from iron ores. Compared with the blast furnace route, coking and iron ore agglomeration (sintering and pelletizing) processes are eliminated which inherently lead to at least 20% reduction of CO_2 emission. This reduction can be further improved, up to 80%, by incorporating carbon capture technologies.

A. Hosseini, E. Georgopoulos, E. Offerman, Y. Yang
Department of Materials Science and Engineering
Delft University of Technology
2628 CN Delft, The Netherlands
E-mail: a.hosseini-1@tudelft.nl

V. Dihman, J. Hage, K. Meijer, C. Zeilstra
R&D Ironmaking
Tata Steel IJmuiden
1951 JZ Velsen-Noord, The Netherlands

The ORCID identification number(s) for the author(s) of this article can be found under https://doi.org/10.1002/srin.202200193.

A pilot-scale HIsarna process has been set since 2010 in the IJmuiden Works of Tata Steel Europe with a capacity of 8 ton h^{-1} of hot metal production. Since then the technology is under development toward industrial demonstration. The main reactor and off-gas system can be divided into five parts, namely, SRV, CCF, reflux chamber, air quench, and up leg as shown in **Figure 1**. Fine iron ore and oxygen are fed into the cyclone convertor furnace (CCF) along with oxygen which combust partly the $CO–H_2$ mixture coming from Smelting Reduction Vessel (SRV). The combustion process provides the necessary heat to prereduce and melt the iron ore. The prereduced and molten iron oxide droplets hit the CCF walls creating a liquid film, which drips along the wall and falls into the molten bath of the SRV.

A set of coal powder injectors are installed in the bath, injecting coal, which is gasified to perform further reduction of the partially reduced iron ore dripping from the CCF walls. Inside the bath the melt is separated into two molten layers which are a top layer of slag and a bottom layer of molten carbonated iron. The emitted gases from reduction reactions in the bath are partially combusted in the top space of SRV by injecting oxygen, which will provide the necessary heat to maintain the required temperature to keep the bath in molten state.

From plant operation data and different trial campaigns, the reactor showed high raw material flexibility and is therefore attractive for processing secondary iron sources. Among the materials that can be recycled through HIsarna is any form of zinc-bearing material such as steel scrap, preprocessed briquettes, etc.

The idea is to inject zinc-bearing material (here steel scrap) into the SRV through an inclined chute depicted in Figure 1. The materials will fall into the hot liquid slag ($T = 1500\,°C$) and immerse in the slag phase. Even though the temperature of particle surface will increase, since the steel particles are made of pure iron and 0.2% carbon, a temperature as high as 1535 °C is needed for melting to take place. The particles will enter molten-carbonated iron phase with around 4% of carbon content. In this phase, the melting temperature for particles, due to carbon diffusion, is as low as 1150 °C. The particles will melt in the liquid iron phase and practically are recycled.

The zinc content of injected particles is vaporized on the slag surface and is concentrated in the escaped dust collected in the
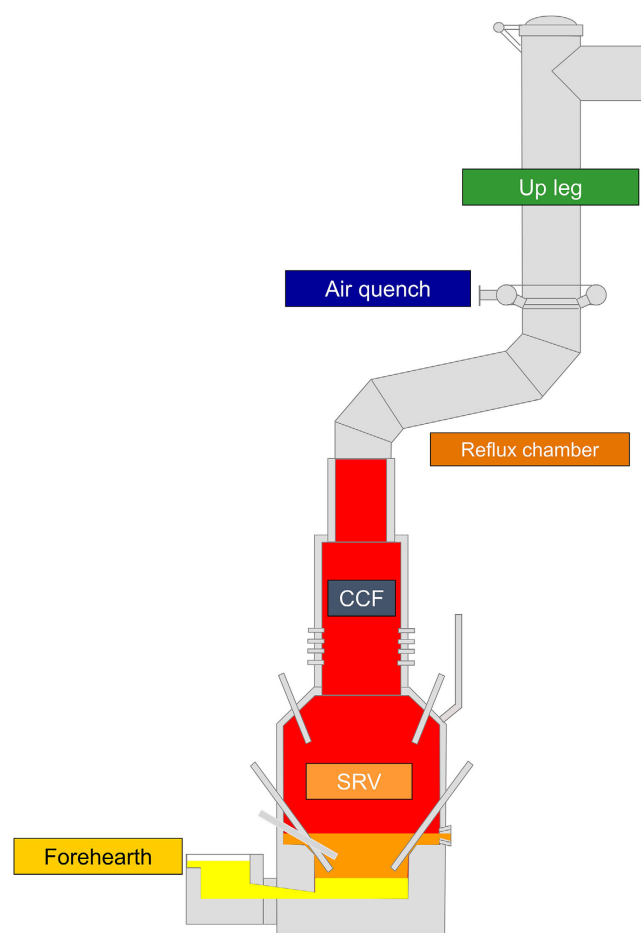
**ADVANCED
SCIENCE NEWS**

www.advancedsciencenews.com

**steel
research**
international

www.steel-research.de

Figure 1. Schematic overview of the HIsarna pilot reactor, including off-gas system.

bag house, which can be recovered in the form of zinc oxide in secondary processes. This flexibility makes HIsarna an interesting secondary resource for extracting zinc from byproducts and waste streams and reusing. The recycling of zinc improves the iron yield of steel production and reduces the need for landfilling, or even opens the possibility to process the contents of existing landfills and tailings, lessening their environmental impacts and contributing to circular economy.

As mentioned before, the material is fed into the SRV using an inclined chute. Proper distribution of the steel particle on the slag surface is crucial for the efficient operation of the furnace since it appears to affect the thermal conditions and surface motion of molten liquid and also zinc vaporization rate from particle surface. The flow behavior of the feeding material in the chute and its velocity at the tip of the chute are factors that significantly affect the distribution of the scrap on the burden surface. Thus, a better understanding of the phenomena occurring during the flow of the scrap along the chute and inside the reactor is required.

In general, the study of granular flow has practical importance in many industrial applications. There have been numerous experimental studies on the behavior of granular material in different shapes, forms, and physical properties. Along with experimental studies, there have been also extensive studies on the

modeling of granular flows. Discrete element method (DEM) has been extensively used to describe granular flows in several small- and large-scale industrial applications. Using DEM modeling, it is possible to analyze the behavior of individual particles in detail to obtain various information and parameters, which is impossible or difficult to observe and measure by experiments. Such information can be effectively used to clarify the mechanisms that control different phenomena and achieve optimized design of operations, equipment, and processes. There have been extensive studies for small-scale applications like in fluidized beds,[1–3] drum mixers,[4–6] hoppers charging and discharging systems,[6–10] and inclined chutes.[11–14]

Wand et al.[15] used DEM modeling to predict the flow behavior of loose cohesive soil. The accuracy of their model is evaluated under different soil moisture contents and by experimentally measuring the slumping angle of repose test and funneling angle of repose test and then comparing with the predictions. They found that the rolling friction coefficient of soil interparticles is increased with moisture content.

In another interesting study, Ganesan et al.[16] developed and calibrated a DEM model to investigate the distribution of powder particles during spreading and densification. Using their validated DEM model, they measured the normal and tangential stress acting on the bottom layer of compacted bed. They concluded that the horizontal compactor results in a higher powder layer quality and that shear stresses is increased with increasing number of particles and compactor speed.

Arifuzzaman et al.[17] used DEM modeling to study the effect of vibration on small particle percolation through a packed bed of large particles under sinusoidal vibration. They validated the developed model with experimental measurements and investigated the effect of vibration amplitude, frequency, and particle size ratios on radial distribution of particles and percolation velocity. They observed that percolation velocity is decreased with an increase in vibration frequency and amplitude when size ratio of small-to-large particles (d/D) is smaller than threshold of 0.154. When the size ratio is larger than the reported threshold, by increasing amplitude and frequency of vibration, the percolation velocity is increased first and then decreased.

Wei et al.[18] developed a DEM model to investigate the distribution of pellet/sinter in blast furnace burden. They have claimed that proper distribution of the particle burden is of outmost importance for the chemical reactions between gas and solid burden. They have investigated the effect of particles shear modulus on the material trajectories and particle distribution in the burden and in radial direction. They have concluded that reducing shear modulus in the developed model can speed up the simulation and lower the costs with a minor or negligible effect on the predicted particle velocities at the chute tip and particle distribution in the burden by measuring and comparing the average, maximum, and minimum velocities of pellets.

In most of the large-scale DEM studies (like the pilot-scale one in this study), the main aim is to reduce the computational cost. Besides the geometry, particle consideration can significantly affect the simulation time. Different methods such as ignoring particle shapes (using only spherical particles), particle upscaling, coarse grain modeling, and periodic simulations have been proposed to reduce the related complexity and computational cost.

For example, Moncada et al.[19] successfully developed and validated a DEM model to predict the performance of a gyratory crusher. The validation was performed in terms of throughput, crushed particle size, and crushing power and the effects of particle size on power consumption, torque force, and equipment fatigue were investigated.

Cleary[20] studied three different cases using DEM analysis. Among the studied case, there was large-scale investigation of dragline and bucket filling for the mining process. In his investigation of this particular equipment, the bucket fill rates and bucket stability were found to be significantly affected by the shear strength and aspect ratio of the particle.

Lommen et al.[21] performed DEM analysis of the large-scale grab equipment used for unloading dry bulk cargo vessels. They derived scaling laws for particle upscaling to reduce the particle numbers and therefore reducing the simulation costs. They concluded that by particle upscaling techniques, it is possible to reduce computational time up to 55 times.

Mikio et al.[22] performed DEM analysis of the large-scale pneumatic conveyer using coarse-grain model, where a modeled particle is considered to have larger size than the original particle and one modeled particle can represent a crowd of original particles. This way, smaller number of particles than the original system is utilized. In both the coarse-grain system and the original one, the simulation results satisfied the relationship between different parameters and agreed well with experimental results such as stationary layer area occupation and the plug velocity while reducing the simulation time drastically.

Morrissey et al.[23] modeled a large scale win-screw granulator. Instead of focusing on particle count reduction, they reduced the computational effort through periodic simulations. Using this approach and careful consideration of periodic boundary conditions, they could capture and reproduce the key particle dynamics and identical behavior of the flow to their counterparts' full-scale simulation.

In the current study, it has been attempted to reduce the computational cost by investigating the effect of particle shape on overall granular flow behavior and to find out if it is possible to ignore the shape of particles, which significantly reduces simulation complexity and cost. This is done through comparison of different calculated parameters with their counterpart's measured value from the experiments for two different approaches. In one approach particles are considered to be spherical and in another one the shape of particles is approximately considered.

A brief overview of the experimental setup, model development, and validation is presented here; however, we would like to refer readers to our previous study for more details.[24]

In this study, the main focus is to apply the DEM model to study the flow of scrap particles into the pilot-scale HIsarna reactor and investigate the effect of different parameters such as chute inclination, injection elevation, injection mode (batch and continuous), batch size and flowrate on particle distribution, and exerted pressure on the liquid slag surface inside the reactor.

2. Pilot Plant Geometry and Simulation Environment

Figure 2 shows the chute position and SRV reactor dimensions. Tip of the chute is placed 3 m above the slag surface (orange surface in Figure 2).

Particles can be released from two different elevations (two different valves namely bottom and top) with height difference of 92 cm, as shown in Figure 2B. The opening speed of each valve is set to $1 \, \text{m s}^{-1}$, which is an average of the experimental measurements. Before running the pilot-scale simulations, a DEM model is developed and validated based on the experimental data. An experimental chute made of Plexiglas, shown in **Figure 3**A, with the same geometry as pilot-scale chute is fabricated to acquire necessary data for model validation. In our previous study,[24] the flowability of steel scrap material with different granular shapes, namely compact, music note, and coupon, is experimentally investigated (Figure 3C). In the current study, a DEM model for compact-shaped scrap is developed and validated based on the experimental data. Below the experimental chute, a box is placed which is divided into nine different slots
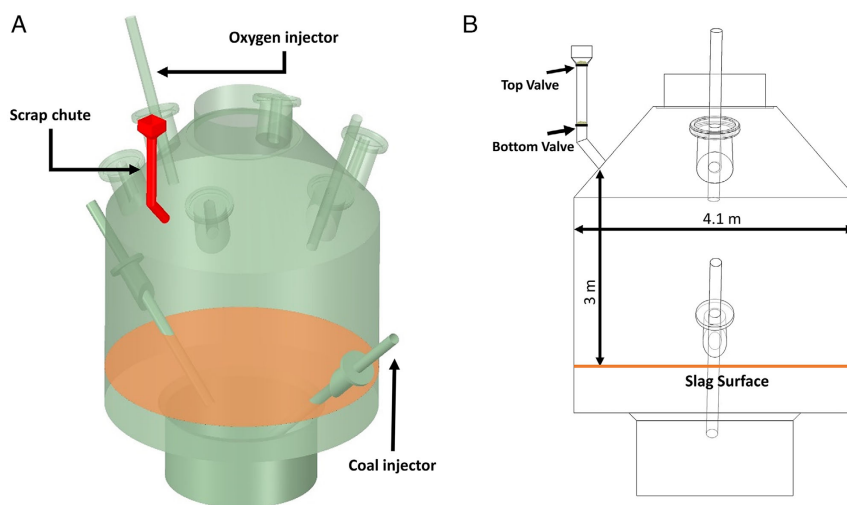
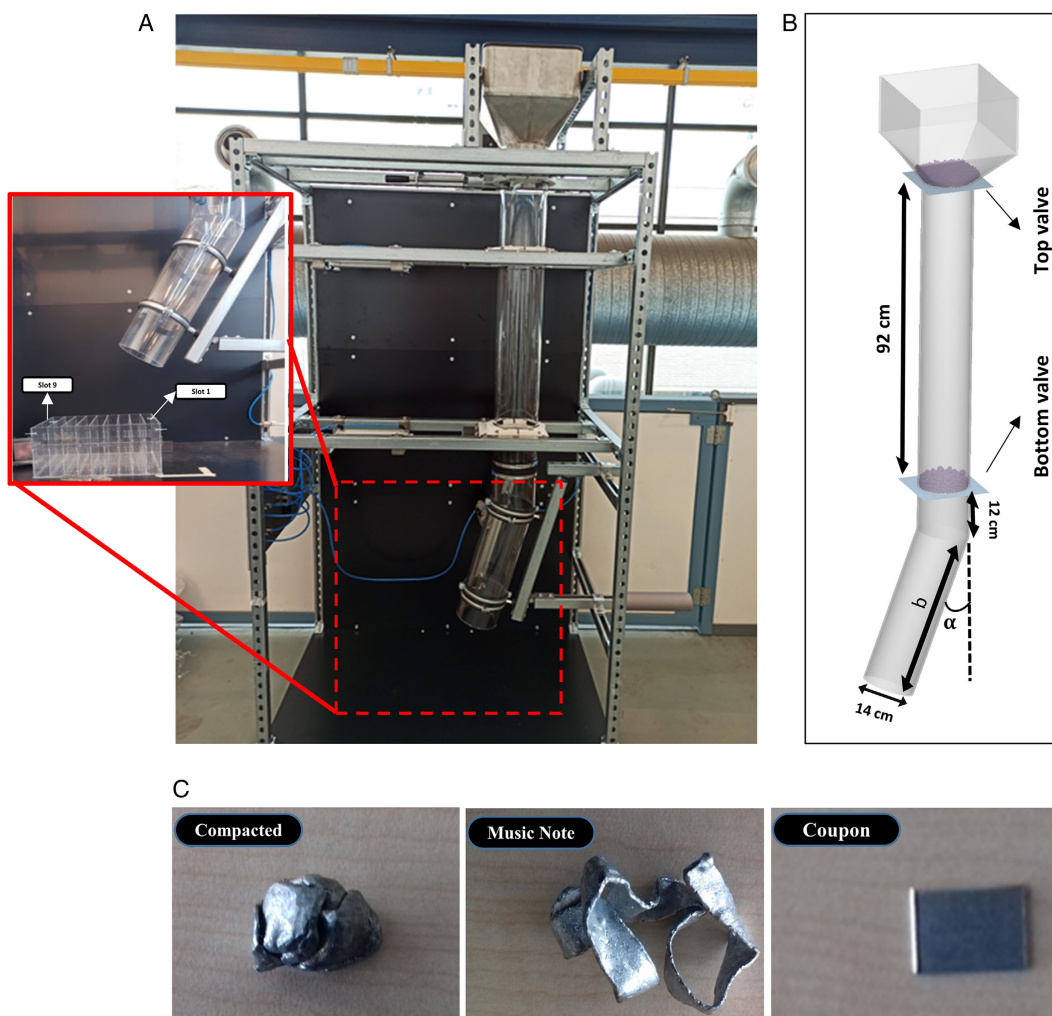**Figure 2.** Schematic view of SRV and dimension used for simulations.

Figure 3. A) The laboratory-scale chute with the sampling box and slot numbers; B) chute geometry with dimensions and C) different types of steel scrap particles.

using walls made of Plexiglas. The chute has an adjustable inclination (α shown in Figure 3B) and is equipped with two different valves at two different elevations. For all performed measurements, particles are released from the lower valve in batch mode (1, 2, and 3 kg) and flow along the chute and after leaving the chute, fall into the sampling box. The average velocity at the tip of the chute (tip velocity) and mass fraction of particles inside each slot are measured for each inclination and batch size which are later used for model validation.

3. Discrete Element Method

EDEM software[25] which uses discrete element method is used to model the granular flow of steel scrap particles. Each particle has six degrees of motion and two types of motion, namely, translational and rotational, which are described through Newton's second law of motion, as stated in Equation (1) and (2) (all of the related equations can be found in EDEM software theory guide[26]).

$$m_i \frac{\mathrm{d}u_i}{\mathrm{d}t} = \sum_{j=1}^{K} (F_{\mathrm{n},ij} + F_{n,ij}^d + F_{\mathrm{t},ij} + F_{t,ij}^d) + m_i g \quad (1)$$

$$I_i \frac{\mathrm{d}\omega_i}{\mathrm{d}t} = \sum_{j=1}^{K} (T_{\mathrm{t},ij} + T_{\mathrm{r},ij}) \quad (2)$$

The mentioned interparticle forces are calculated based on the soft sphere approach where particles are allowed to slightly overlap in both normal and tangential directions. Based on values of overlap, different contact models are available which are composed of spring and dashpot, that correspond to the elastic and plastic nature of particles in the normal direction, respectively, and a slider, spring, and dashpot for the tangential direction, as illustrated in **Figure 4**. In this study, Hertz–Mindlin model with relative velocity-dependent (RVD) rolling friction is used for the contact model.

Detailed formulations of the parameters for Equation (1) and (2) are reported in **Table 1**.

Particle positions are updated by an explicit method after each time step by calculating related torques and forces.[26]
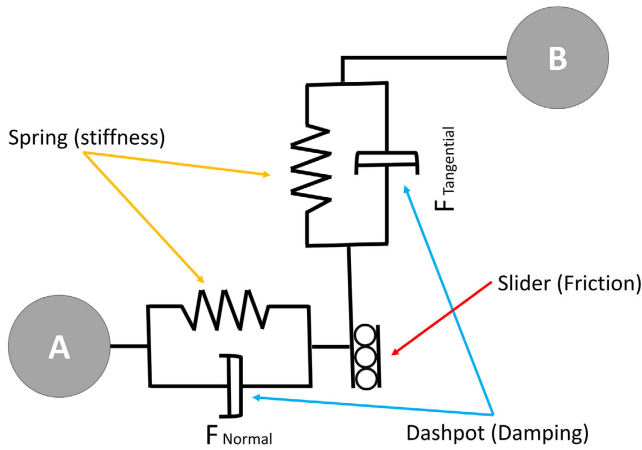
2200193 (4 of 14)

Figure 4. Schematic view of spring and dashpot for contact force modeling.

4. DEM Model Setup

Scrap particles in compact form vary drastically in shape and size. However most of the particles are highly compact and close to spherical shape, as shown in **Figure 5**A. To include the particle size distribution, one kilogram of scrap samples is taken from the plant and particles are divided into six size classes based on the similarities in particles' approximate dimension. Each size group contains particles with approximately the same particle size but various particle shapes.

Using classified particles, it is possible to consider two approaches for particle modeling.

In one approach, the model is set up by considering all particles in spherical form (spheric model). To obtain size distribution for this approach, the number of particles for each size

classes are counted and based on the mass of each class, the equivalent spherical diameter is calculated and used in the simulations, as reported in **Table 2**.

In another approach, the shape of particles is modeled (shaped model) by considering six differently shaped classes which frequently appear inside the batch sample illustrated in Figure 5B. Based on the experimental observations, large particles displayed limited variety in particles shape but wider shape variations are observed for smaller-sized classes. For example, in size class A, all of the shape classes are observed while for size class F only oval, rectangular, and triangle shape classes existed. The result of this observation is reported in the last column of Table 2.

In the DEM model, the real shape of particles is approximated based on the multiple overlapping spheres, forming a cluster close to the real shapes, as indicated in Figure 5C. Different shapes are incorporated into each size classes with an equal mass ratio for each existing shape class.

Considering these two approaches, and also material properties and tuned interaction coefficients listed in **Table 3**, the model is set up and simulations are performed using Euler time integration with a time step of 10^{-6} s and domain cell size equal to three times of particle minimum radius.

For pilot setup, the simulation environment is set just below the slag surface and once the particles hit the slag surface, they disappear from the computational domain. The same Euler time integration with a time step of 10^{-6} s and the same domain cells size equal to three times of particle minimum radius is considered for all simulations. All simulations are performed on a PC with Core i7-6700HQ CPU where six processors are used for parallel computation.

In all cases, the effect of gas flow coming from the reactions inside the liquid slag and also the slag surface motion is not modeled. To consider gas/solid interaction, coupling of EDEM with CFD software such as Ansys Fluent is needed, which is not

Table 1. Mathematical formulations of different terms in force balance equation.

Term	Equation	Parameters
Normal force	$F_{n,ij} = \frac{4}{3} E^* \sqrt{R^*} . \delta_n^{1.5}$	$E^* = \frac{1}{(1 - \vartheta_i^2 / E_i) + (1 - \vartheta_j^2 / E_j)}$
		$R^* = R_i R_j / (R_i + R_j)$
Normal damping force	$F_{n,ij}^d = -2\sqrt{\frac{5}{6}} . \beta . \sqrt{S_n m^*} . v_{ij}^{rel}$	$m^* = \left(\frac{1}{m_i} + \frac{1}{m_j} \right)^{-1}$
		$\beta = \frac{\ln e}{\sqrt{\ln^2 e + \pi^2}}$
		$S_n = 2.E^* \sqrt{\delta_n R^*}$
Tangential force	$F_{t,ij} = -\delta_t S_t$	$S_t = 8G^* \sqrt{\delta_n R^*}$
Tangential damping force	$F_{t,ij}^d = -2\sqrt{\frac{5}{6}} . \beta . \sqrt{S_t m^*} v_{t,ij}^{rel}$	–
Tangential torque	$T_{t,ij} = R_i(F_{t,ij}^d + F_{t,ij})$	–
Rolling friction torque	$T_{r,ij} = -\mu_r F_{n,ij} R^* \hat{\omega}_{rel,ij}$	$\hat{\omega}_{r,ij} = \hat{n}_{ij} \times \frac{v_{t,ij}}{|v_{t,ij}|}$
		$v_{t,ij} = \begin{cases} -\frac{1}{2}(\omega_i + \omega_j) \times \vec{r}_{ij}, & \text{article} - \text{particle contacts} \\ -R_i \omega_i \times \hat{n}_{ij}, & \text{particle} - \text{geometry contacts} \end{cases}$

ADVANCED
SCIENCE NEWS
www.advancedsciencenews.com

steel
research
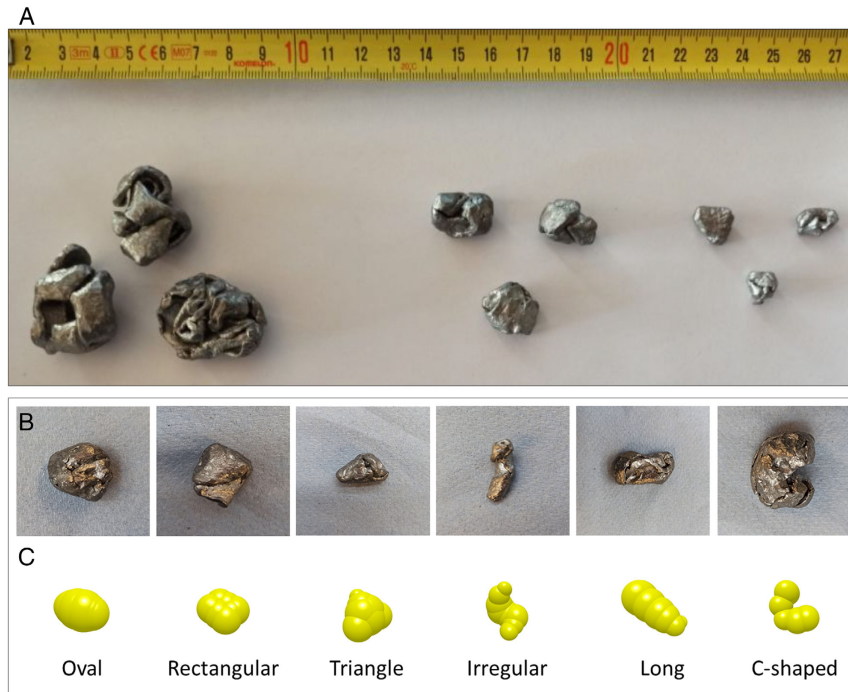international
www.steel-research.de

Figure 5. A) Compact scrap-dominant shapes and size variations, B) considered shape classes, and C) equivalent representation for multiple-sphere approach in DEM.

Table 2. Particle classification and size calculations for spherical approach.

Size class	Equivalent spherical diameter [cm]	Number of particles [for 1 kg sample]	Mass fraction	Existing shape class
A	0.6354	210	0.2	All
B	0.704	52	0.07	Long
C	0.7854	65	0.13	Oval–rectangular–triangle–irregular
D	0.9779	71	0.25	Oval–rectangular–triangle–irregular
E	1.2797	22	0.19	Oval–rectangular–triangular
F	1.661	7	0.13	Oval–rectangular–triangular
Total Batch	0.8344	427	1	–

Table 3. Material properties for Plexiglas and steel particles used in simulations.

Steel Particles		
Density	7800	Kg m^{-3}
Poisson ratio	0.25	–
Shear modulus	7.60 E + 10	Pa
Particle-particle static friction coefficient	0.4	–
Particle-particle rolling friction coefficient	0.05	–
Particle-particle restitution coefficient	0.6	–
Plexiglas		
Density	1200	Kg m^{-3}
Poisson ratio	0.4	–
Shear modulus	8.93 E + 08	Pa
Particle versus Plexiglas static friction coefficient	0.3	–
Particle versus Plexiglas rolling friction coefficient	0.05	–
Particle versus Plexiglas restitution coefficient	0.5	–

possible for this study due to limited computational resources. CFD–DEM coupling is the subject of another study by the same author which is under progress at the moment of writing this paper.

5. Result and Discussion

5.1. DEM Model Validation

Figure 6 shows the mass fraction of particles collected in the sampling box (inclination 20° only, for brevity) and velocity at the tip of the chute (for all inclinations) predicted by the model

for both spherical and shaped approaches. The model is in excellent agreement with experiments and the overall behavior of the particles is very well predicted. No considerable difference was found for two approaches regarding shape considerations, except for differences in angular velocity (not shown here).[24] This is a quite interesting finding since by considering the shape of particles, it is required to include more than one spherical particle to constitute a single particle. For example, five spherical particles
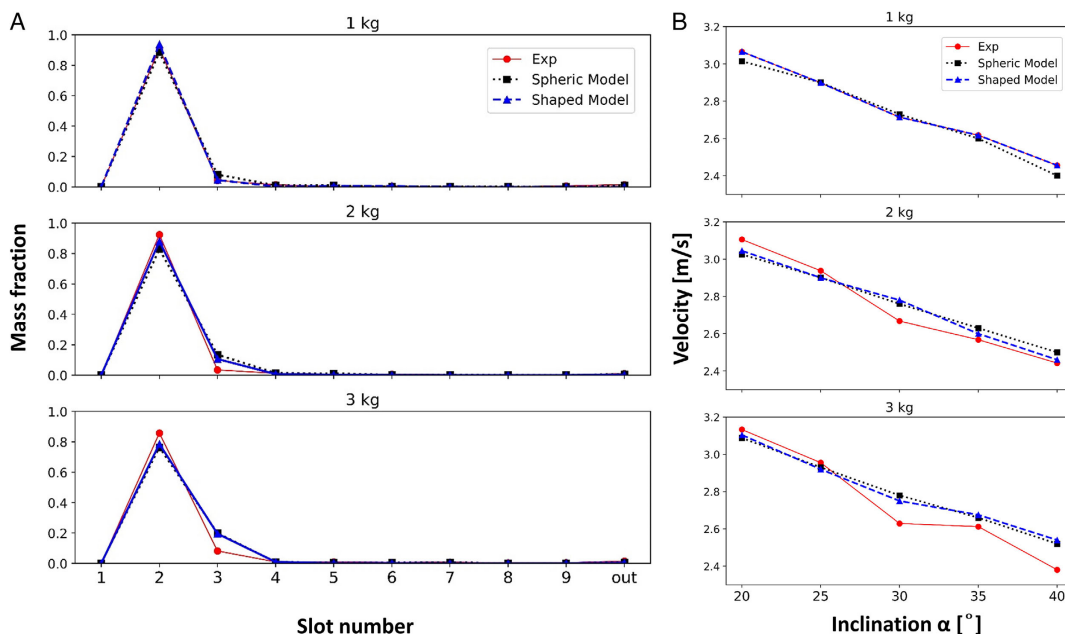
**ADVANCED
SCIENCE NEWS**

www.advancedsciencenews.com

**steel
research**
international

www.steel-research.de

Figure 6. Mass fraction distributions of steel particles in the sampling box for inclination 20° and different A) batch sizes and B) tip velocity for both experiment and calculation—spheric versus shaped model approach.

are required to constitute one single C-shaped particle (shown in Figure 5C). Incorporating higher number of particles can drastically increase the simulation time.

For instance, 3 Kg batch of scrap contains 1281 spheric particles and it takes 20 min to complete a single simulation (using four parallel processors). Considering particle shapes and for the same number of nonspherical particles, ≈6300 spheric particles need to be included which increases the simulation time by a factor of ≈4 using the same processing cores and model settings. The increase in simulation time is more pronounced for larger geometries and simulation environments.

Based on the model predictions and comparisons with experimental data, it can be concluded that the shape of particles can be ignored to reduce the computational cost. Therefore in this study, each scrap piece is represented by single spherical particles with an equivalent diameter for all pilot-scale cases.

Also in real plant operation, the scrap chute is made of steel; therefore, the properties of steel (physical properties and interaction coefficient) for both particles and chute material are used.

5.2. Batch Mode Injection of Particles

At current plant operation, the scrap particles are injected in batch mode (3 kg) with a fixed inclination angle. Particles are loaded from top and accumulated on top of the valves. Once the mass of particles reaches 3 kg, the loading is stopped, valves are opened, and the batch of material is fed into the SRV all at once. This process is repeated in fixed intervals to meet a feeding rate of 2 ton h^{-1}. In this section, the effect of chute inclination, release elevation, batch size, chute length (length b in Figure 3B) on the position of particles, and exerted pressure on the slag surface are investigated.
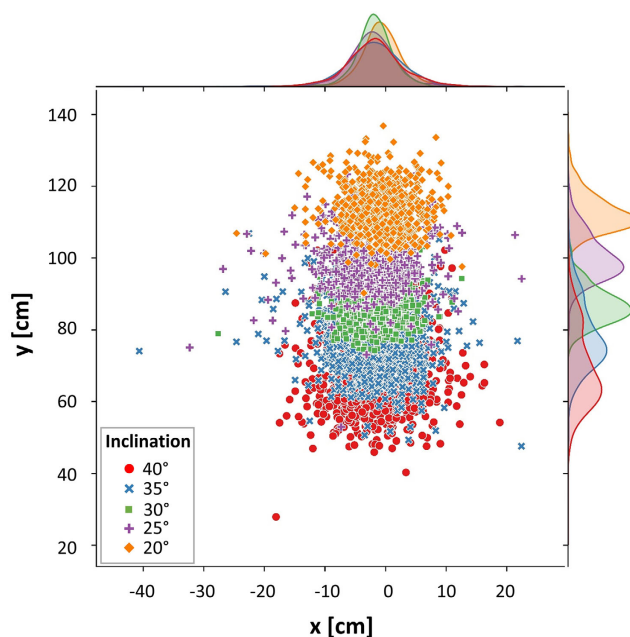

Figure 7. Scatter plot of particles position on the slag surface with distributions in x and y directions - different inclinations (bottom valve).

5.2.1. Effect of Chute Inclination

Initially, the materials are injected into the SRV from bottom valve and in batch size of 3 kg.

Figure 7 shows the scatter plot of particles position hitting the slag surface with respect to the SRV cross section (x and y ranges are from −200 to 200 cm). As shown, for all investigated

inclinations, the particles hit the surface within the distance of wall and center of the SRV. Paticles are thrown further toward the center by increasing the chute inlination (α). The aim is to avoid pouring high concentrations of particles in the middle of the slag surface ($x = 0$ and $y = 0$ coordination) and also avoiding the near-wall region. At the center, due to the gas/solid injection inside the slag phase, a fountain is formed. It is preferred to avoid disturbing the fountain since it could be detrimental to the function of coal injection ports.

On the same figure, particles distribution curves on the axes in x and y direction are also shown. The distribution graph in both directions is slightly flatter by increasing the inclination. Higher inclination reduces the particle velocity and gives more time for particles to segregate from each other while flowing over the inclined part of the chute. However, they are still highly concentrated with a sharp peack in the middle of the occupied area and increasing the inclination does not have a considerable effect on particle distribution. In order to have a more quantified analysis, the approximate occupied area by particles is manually calculated based on the sketch depicted in **Figure 8**A. This area will be called

"impact area" hereafter and refers to the area occupied by particles ($A_{particles}$) over total slag surface ($A_{slag\ surface}$).

$$\text{Impact area}(\%) = \frac{A_{particles}}{A_{slag\ surface}} \times 100 \qquad (3)$$

The quantified values for impact areas are shown in Figure 8B for different inclinations.

There are three reasons to prefer larger impact area (flatter particle distribution graph) over the slag surface. Once particles are poured into the liquid slag, due to high slag viscosity, they tend to decelerate before immersing into the slag phase. This causes accumulation of particles on top of each other and creating a mountain of material for a small fraction of time. Accumulated material reduces the local temperature of the slag surface and might cause local liquid freezing.

Figure 9A, shows experimental observations of slag temperature once 2 kg of steel scrap is poured into a static slag surface. The experiment is performed at laboratory scale by CRM group.[27] As shown, initially the temperature of the slag surface
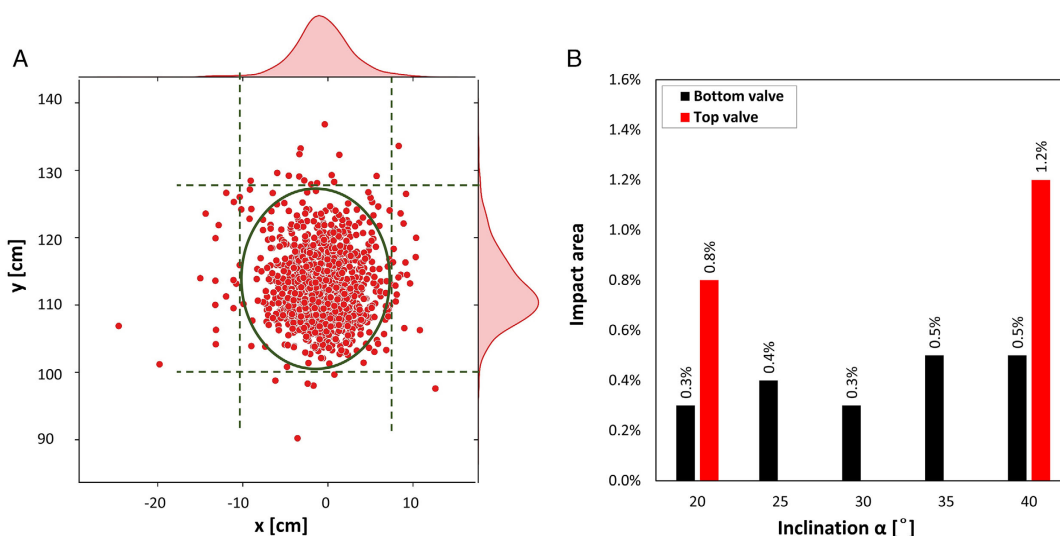

Figure 8. A) Approximate particles impact area and B) calculated impact area for different inclination.
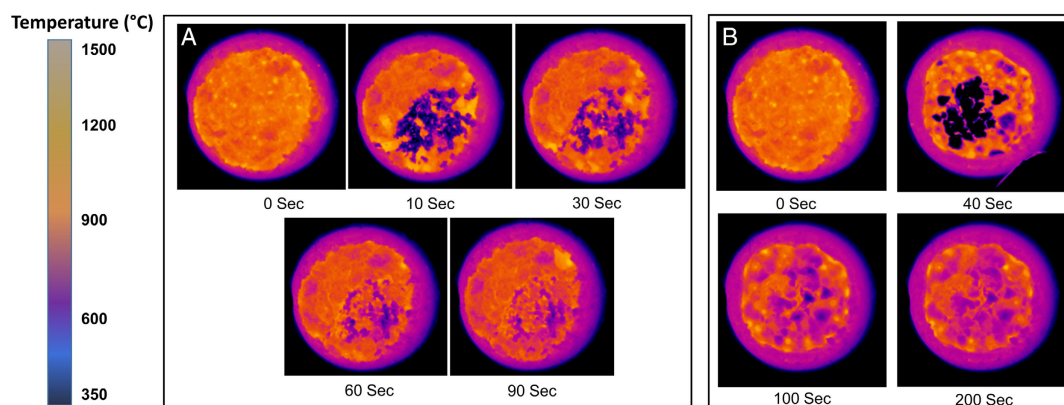

Figure 9. Slag temperature contour for A) 2 kg zinc-coated scrap and B) 0.5 kg briquettes addition.

is uniform (except for the near-wall region where cooling occurs). Once particles are poured into the surface, they float on top and the local temperature is highly reduced and is then slowly recovered. The temperature recovery takes at least 90 s when injecting scrap particles and can be increased to 200 s once briquettes with bigger sizes and denser structures are added, as shown in Figure 9B.

The second reason that makes larger impact areas more desirable is the effect on zinc vaporization from the particles. The zinc content needs to be evaporated, preferably during flying time or on the slag surface. As mentioned before, once a batch of particles hits the surface, they tend to create a mountain of material and this accumulation can lower the rate of zinc vaporization from particles, especially those at the bottom of the batch. With a wider spread of particles (larger impact area), higher particle surface will be available, which increases vaporization rate of zinc from the individual particle surface into the gaseous phase. Lowering the vaporization rate will give zinc element more chance to speciate into the slag phase which is undesired.

The last reason to aim for larger impact area is the liquid slag splashing height. When particles with a high concentration hit a small area on the slag surface, they exert a significant pressure in a short time interval and could cause splashing of the liquid slag. These splashes can reach the sidewalls at the top and might also hit the chute outlet and block it. This phenomenon has been reported in previous pilot-scale trials, and almost any time scrap is injected in batch mode.

All of the mentioned issues can be addressed if particles are distributed over a larger area on the slag surface. So a comprehensive study is performed to investigate an effective strategy to flatten the particle distribution curve when particles are injected in batch mode.

The results presented for batch mode released from the bottom valve (Figure 7 and 8) will be used as a base case for all comparisons.

5.2.2. Effect of Elevation

A set of simulations for inclination angles of $\alpha = 20°$ and $40°$ is performed where particles are released from the top valve.

As shown in **Figure 10**A, the distribution of particles over the slag surface is more uniform and impact area is larger once particles are released from a higher elevation (≈ 2.7 times larger area for both inclinations, as reported in Figure 8B). As particles are released from the top valve, there is more time for particle separation while falling in the vertical section of the chute. Separated particles hit the surface of the inclined section with higher velocity to segregate even more at the chute tip, as shown in Figure 10B. Also due to a higher velocity at the tip, particles travel further and land closer to the center.

Figure 11 shows the impact pressure, defined as total force divided by final impact area, exerted by mass of particles on the slag surface from time the first particle hits the surface (impact time). As shown, the impact pressure is much lower for top valve mainly due to a larger impact area. It is possible to relate the pressure to the slag liquid splash caused by particles hitting the surface. The higher the impact pressure, the higher the risk of liquid splashing.

5.2.3. Effect of Batch Size

For chute inclination of 20°, different batch size is injected from the bottom valve to see how particle distribution and impact pressure might be affected. There is a slight change in the impact area as the batch size is increased, however, with sharper distribution curve due to higher number of particles and higher exert pressure, as shown in **Figure 12**. This is because the number of particles hitting the surface at the same time interval is increased for higher batch sizes which could increase the risk of liquid splashing. Heavier batches could also absorb more heat so there will be a higher temperature disturbance at the slag surface. Based on this observation, once batch mode is used, it is
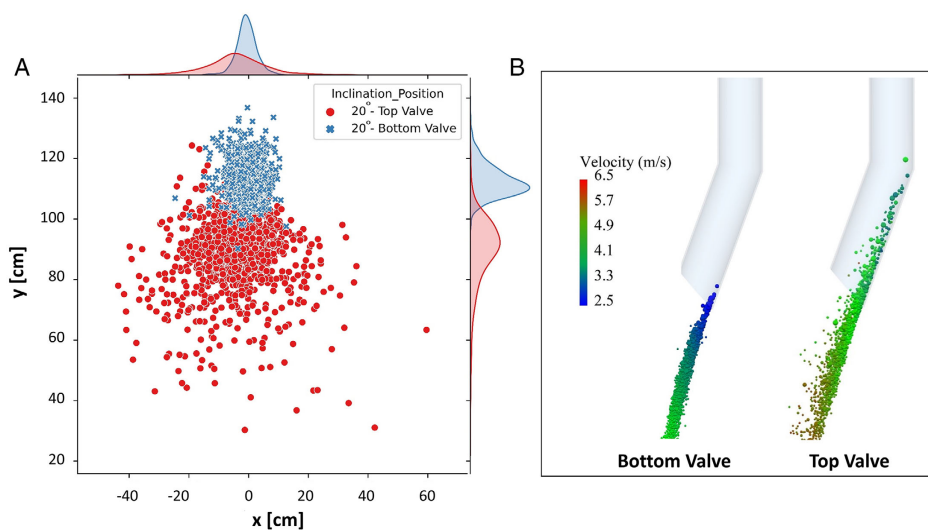
Figure 10. A) Scatter plot of particles position on slag surface and B) particle flow colored by velocity after leaving the chute for batch mode and inclination 20°—top and bottom valve.
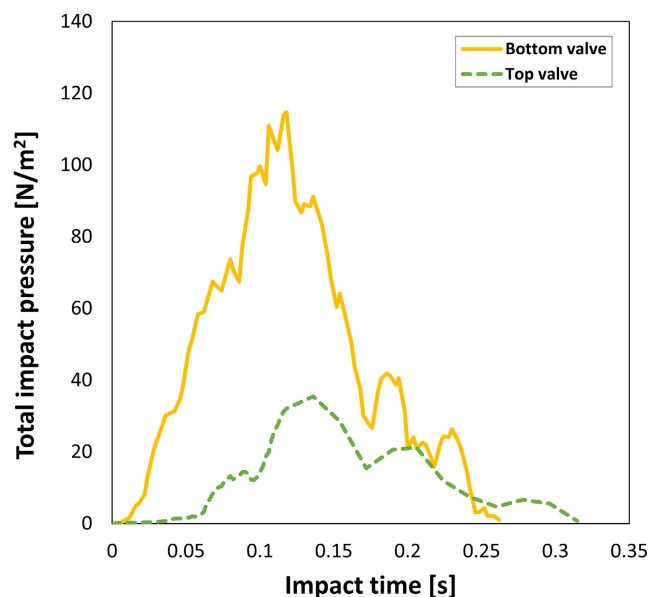
Figure 11. Impact pressure on the slag surface for batch mode and inclination 20°—top and bottom valve.

Figure 13. Effect of chute length on particle position on slag surface for inclination 20°.

suggested to inject particles in smaller batch sizes. The same behavior was observed for top valve injection; however, the results are not shown here for brevity.

5.2.4. Effect of Chute Length

For fixed inclination of 20°, two more simulations are performed where the length of the inclined section (length b in Figure 3B) is doubled to see the effect on flow behavior. It is important to see the effect of this parameter as in some cases it will be necessary to increase the length to position the vertical part of the chute away from the CCF and SRV outer walls to provide enough space for maintenance.

As shown in **Figure 13**, for shorter length (short tip), particles are still agglomerated and flow as a bump-shaped batch which
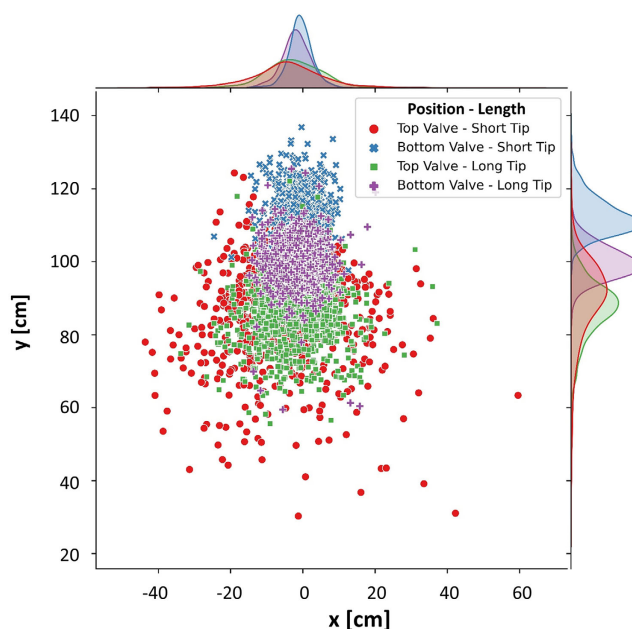
causes lower velocity at the tip of the chute. Using a longer length (long tip), particles are elongated more before reaching the tip. This elongation gives particles more time to spread from each other in the flow direction and due to longer distance, particles have more time to accelerate to get higher tip velocity. With higher tip velocity, particles land closer to the center of the slag surface, which is more pronounced for the top valve. Longer length also slightly reduces the impact area on the surface but the difference with shorter length is negligible.

5.2.5. Effect of Dent-Shaped Obstacles

So far, the investigated parameters have not led to any considerable increase in impact area or reduction in exerted pressure.
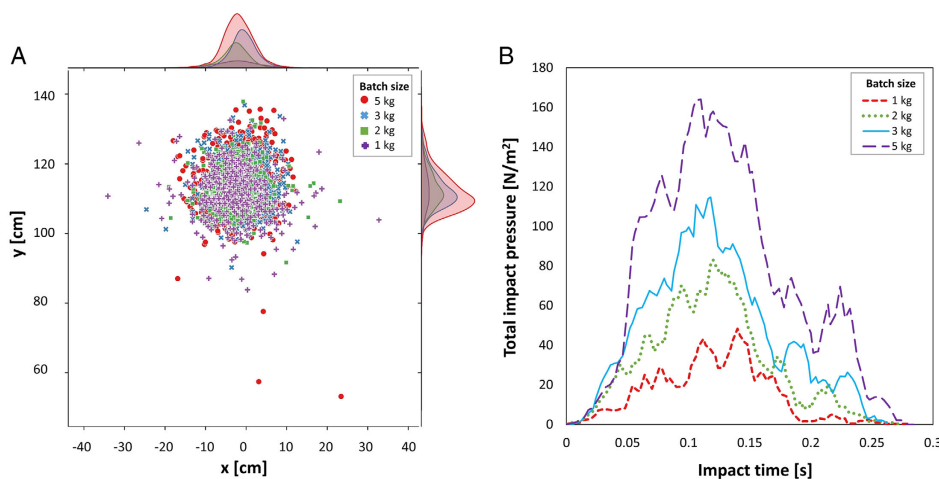

Figure 12. A) Effect of batch size on particle position and B) impact pressure for inclination 20°: bottom valve.
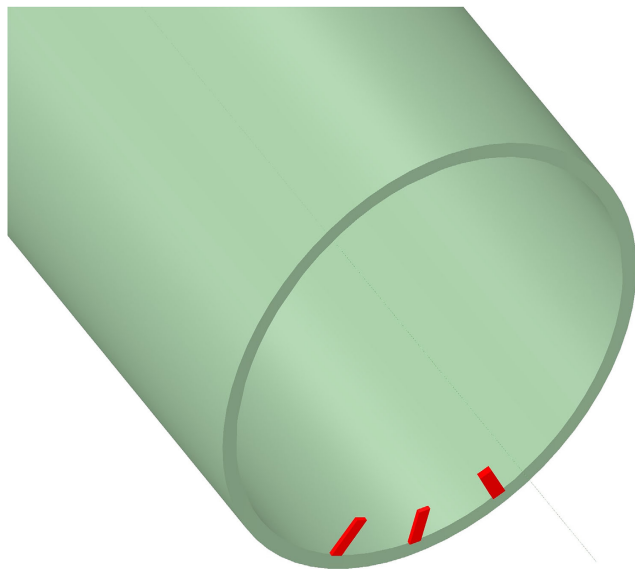
**ADVANCED
SCIENCE NEWS**

www.advancedsciencenews.com

**steel
research**
international

www.steel-research.de

Figure 14. Obstacles' position on the tip of the chute.

after the particle batch leaves the chute. The quantified impact area for top and bottom valve is shown in **Figure 16**B.

Larger impact area in turn reduces the impact pressure on the slag surface, as depicted in Figure 16A, for inclination of 20°. This reduction is more pronounced once the batch of particles is released from the top valve.

5.2.6. Effect of Obstacle Dimension

The obstacle height for initial simulations was fixed to 15 mm. It is desired to reduce the height of obstacles since longer dents are imposed to more erosion and wearing as particles are hitting them on their flow path. The effect of obstacle height on particle pattern on the slag surface is reported in **Figure 17**A. As the heights of obstacles are reduced, the particle distribution becomes more concentrated and closer to the case without obstacles with a reduced impact area and increased pressure on the surface. However, as illustrated in Figure 17B, even an obstacle with a very small height (2.5 mm) can have a considerable effect on particle distribution and impact area compared with the case without obstacles (minimum ten times larger impact area).

5.3. Continuous Mode Injection of Particles

Another possible method for particle injection into the SRV reactor is continuous feeding mode with an adjustable flowrate. A set of simulations for inclination 20° is performed where a batch of 3 kg is injected into the SRV from the bottom valve with flowrate of 2 ton h^{-1} (0.56 kg s^{-1}), which is the same flowrate for scrap injection in the real plant operation.

According to **Figure 18**A, feeding particles with continuous mode can have a noticeable effect on the impact area and distribution pattern on the slag surface. The major change is a flatter distribution curve in x-direction compared with the batch mode.
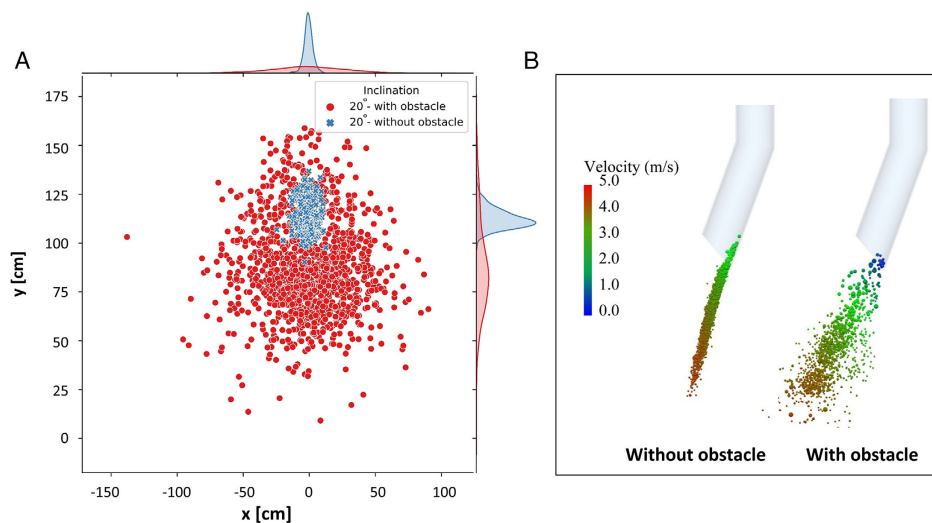
However, one interesting approach that can flatten the distribution and impact pressure curve is to place small dent-shaped obstacles at the tip of the chute, as shown in **Figure 14**. The obstacles are aligned with tip cross section and placed along the internal circumference with a fixed height of 15 mm.

Once particles hit the obstacles, they are stalled and create a temporary barrier that make rear particles slide over the barrier to create a wider particle flow. Ultimately particles hit the slag surface, creating a significantly larger impact area and flatter particle distribution curve, as illustrated in **Figure 15**A. Higher spread of particles once obstacles are placed at the tip is clearly visible from Figure 15B, which depicts the track of particles right

Figure 15. Scatter plot of particles position on A) slag surface and B) particles flow colored by velocity after leaving the chute for batch mode and inclination 20°: bottom valve with/without obstacle.
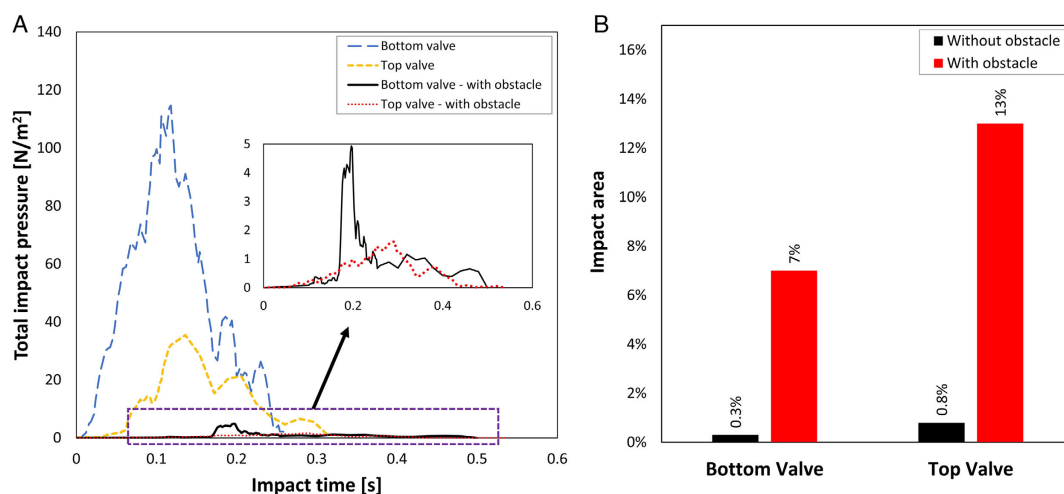
2200193 (11 of 14)

ADVANCED
SCIENCE NEWS

www.advancedsciencenews.com

steel
research
international

www.steel-research.de

Figure 16. A) Impact pressure on the slag surface and B) calculated impact area for inclination 20° and top and bottom valve: with/without obstacle.
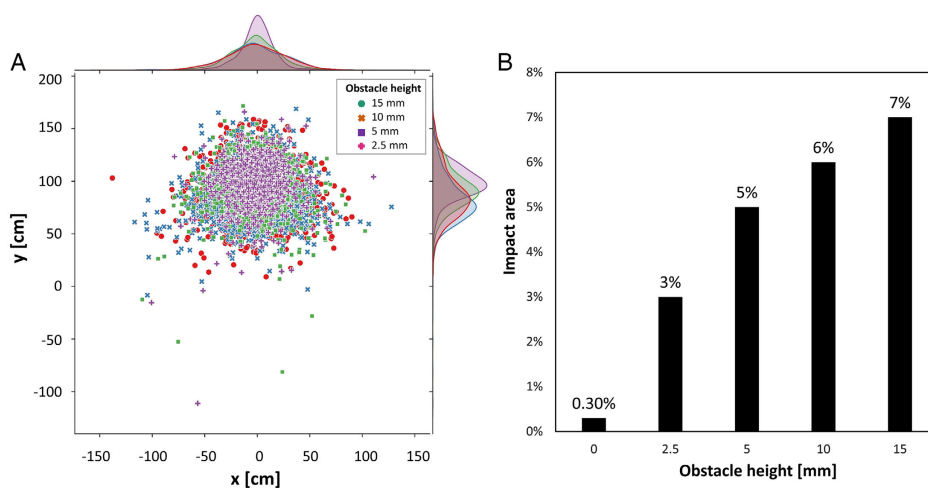

Figure 17. A) Effect of obstacle tip height on particles position on slag surface and B) calculated impact area for batch mode and inclination 20°.
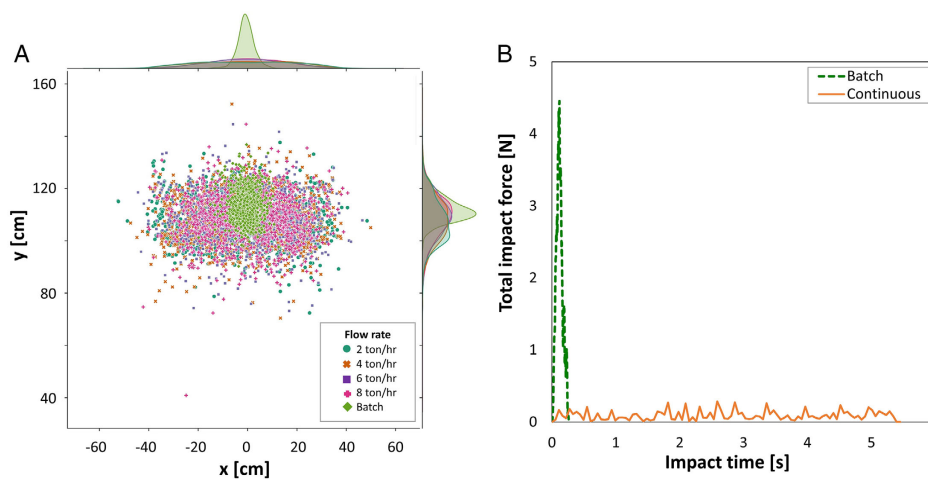

Figure 18. A) Scatter plot of particles position for batch mode and continuous mode on slag surface and B) impact force for batch and continuous mode of 2 ton h^{-1}.

**ADVANCED
SCIENCE NEWS**

www.advancedsciencenews.com

**steel
research**
international

www.steel-research.de

This trend is the same for all inclinations and for both top and bottom valves.

Beside larger impact area, continuous injection offers another benefit. In batch injection, the whole mass of particles hits the slag surface in a very short time interval (0.3 s for inclination 20° and batch size of 3 kg), with a very high flowrate, which causes a sharp peak of impact force, as shown in Figure 18B. However, in continuous mode, considering the same amount of injected mass, particles are fed in a longer time period (5.3 s for 3 kg batch with flowrate of 2 ton h^{-1}) to distribute the same force over longer time, causing a substantial reduction in impact force on the surface, as shown in the same figure. If the impact area is considered, the impact pressure is even lower compared with the batch mode.

In another set of simulations, the effect of flowrate for continuous mode is investigated, where 3 kg of particles are injected with four different flowrates (2, 4, 6, and 8 ton h^{-1}). As shown from the same figure, there is no specific difference in particle pattern over slag surface for different flowrates and injection with any flowrate will lead to a larger impact area compared with the batch mode. However, higher flowrate can increase the impact force on the slag surface.

6. Conclusion

A comprehensive study has been performed to model steel scarp injection into the HIsarna reactor. A DEM model is developed and validated using experimental data. From the calculations it was concluded that for the current system, the effect of particle shape can be ignored in the models which could substantially increase the calculation speed. Using the final validated model, a combination of different chute inclination, injection height, injection mode, injection size, and flowrate on particle distribution and exerted pressure over the slag surface are studied and the following conclusions are derived for different injection modes.

6.1. Batch Mode

1) Higher inclination angles make particles land more toward the center of the slag surface; however, up to 40° they will not reach the center where the formed fountain by gaseous injection is. 2) Higher inclination angles lead to slightly larger impact area on the slag surface and particle distribution cure is flatter (higher spread of particles over the surface). 3) Releasing particles from higher elevation leads to a larger impact area by particles and with a flatter curve for particle distribution (higher spread of particles over the surface). 4) Positioning small dent-shaped obstacles at the tip of the chute can significantly flatten the particle distribution cure and increase the impact area on the slag. This will lead to noticeable reduction in impact pressure on the slag surface. 5) Longer tip length (length b in Figure 3B) has no major impact on impact area and distribution curve, but it increases the tip velocity of the particles which causes particles to land closer to the center of the slag surface. 6) Higher batch sizes have a negligible effect on the impact area but can significantly increase impact pressure on the surface, thus increasing the risk of liquid splash.

6.2. Continuous Mode

1) Compared with batch mode, continuous mode increases the separation of particles on the slag surface to flatten the distribution cure especially in x-direction of the shown plots. 2) The forces on slag surface are distributed over a longer time interval for continuous mode, leading to a steady curve without any peak. Since particles are injected in a uniform manner with smaller portions, the risk of splashes caused by particles is highly reduced. 3) Higher flowrates will have a minor effect of distribution curve; however, it can lead to higher pressure on the slag surface. Nevertheless, for any flowrate there will be much lower pressure exerted on the slag surface and lower risk of splash compared with batch mode.

Considering the obtained results and derived conclusions, it was suggested to inject the particles with continuous mode of injection with low chute inclination in the range of 20°–30°. By implementing this strategy during recent plant operations, no splashing or specific temperature disturbance has been reported. So it seems dosing particles with continuous mode is the best solution to address problems encountered during batchwise injection. However, batchwise injection must be always considered when continuous injection is not possible due to technical difficulties during the operation to keep the process steady. In this case it is suggested to inject the particles in small batches or larger batches using dental-shaped obstacles at the tip of the chute to reduce impact pressure and temperature disturbance on the slag surface. This is also beneficial to obtain higher rate of zinc evaporation from the particle surface. So proper knowledge of both injection modes seems to be vital to ensure smooth and steady operation.

Conflict of Interest

The authors declare no conflict of interest.

Data Availability Statement

The data that support the findings of this study are available from the corresponding author upon reasonable request.

[1] W. Peng, Y. He, T. Wang, *Adv. Powder Technol.* **2014**, *25*, 896.
[2] H. A. Khawaja, *J. Computat. Multiphase Flows* **2015**, *7*, 227.

[3] L. Zhou, L. Zhang, L. Bai, W. Shi, W. Li, C. Wang, R. Agarwal, *RSC Adv.* **2017**, *7*, 12764.

[4] R. K. Soni, R. Mohanty, S. Mohanty, B. K. Mishra, *Adv. Powder Technol.* **2016**, *27*, 531.

[5] Y. Xu, C. Xu, Z. Zhou, J. Du, D. Hu, *Particuology* **2010**, *8*, 141.

[6] P. W. Cleary, M. L. Sawley, *Appl. Math. Model.* **2002**, *26*, 89.

[7] A. Anand, J. S. Curtis, C. R. Wassgren, B. C. Hancock, W. R. Ketterhagen, *Chem. Eng. Sci.* **2008**, *63*, 5821.

[8] J. Qiu, D. Ju, J. Zhang, Y. Xu, *Powder Technol.* **2017**, *314*, 218.

[9] H. Tangri, Y. Guo, J. S. Curtis, *Chem. Eng. Sci. X* **2019**, *4*, 100040.

[10] G. Degrassi, L. Parussini, M. Boscolo, N. Petronelli, V. Dimastromatteo, *SN Appl. Sci.*, **2021**, *3*, 242.

[11] Y. W. Yu, H. Saxén, *Ironmaking Steelmaking* **2011**, *38*, 432.

[12] H. J. H. C. Sushil, S. Shirsath, J. T. Padding, J. A. M. Kuipers, T. W. J. Peeters, *AIChE J.* **2014**, *60*, 3424.

[13] H. Mio, S. Komatsuki, M. Akashi, A. Shimosaka, Y. Shirakawa, J. Hidaka, M. Kadowaki, S. Matsuzaki, K. Kunitomo, *ISIJ Int.* **2008**, *48*, 1696.

[14] Y. Yu, H. Saxén, *Ind. Eng. Chem. Res.* **2012**, *51*, 7383.

[15] X. Wang, Q. Zhang, Y. Huang, J. Ji, *Biosyst. Eng.* **2022**, *215*, 283.

[16] V. V. Ganesan, A. Amerinatanzi, A. Jain, *Powder Technol.* **2022**, *405*, 117557.

[17] S. M. Arifuzzaman, K. Dong, H. Zhu, Q. Zeng, *Adv. Powder Technol.* **2022**, *33*, 103551.

[18] H. Wei, Y. Zhao, J. Zhang, H. Saxén, Y. Yu, *Adv. Powder Technol.* **2017**, *28*, 2482.

[19] M. Moncada, P. Toledo, F. Betancourt, C. G. Rodríguez, *Minerals* **2021**, *11*.

[20] P. W. Cleary, *Powder Technol.* **2000**, *109*, 83.

[21] S. Lommen, M. Mohajeri, G. Lodewijks, D. Schott, *Powder Technol.* **2019**, *352*, 273.

[22] M. Sakai, S. Koshizuka, *Chem. Eng. Sci.* **2009**, *64*, 533.

[23] J. P. Morrissey, K. J. Hanley, J. Y. Ooi, *Pharmaceutics* **2021**, *13*, 2136.

[24] E. Georgakopoulos, A. Hosseini, T. Kerry, J. Hage, K. Meijer, E. Offerman, Y. Yang, *Steel Res. Int.* **2022**, *93*, 2200075.

[25] EDEM Software, https://www.altair.com/edem, (accessed: June 2022).

[26] DEM Solutions Ltd, EDEM 2.6 Theory Reference Guide. 2014, 2004.

[27] CRM-Belgium, https://www.crmgroup.be/en, (accessed: February 2022).